

# Tailoring Spatiotemporal Light Confinement in Single Plasmonic Nanoantennas

Tobias Hanke,<sup>†</sup> Julijan Cesar,<sup>†</sup> Vanessa Knittel,<sup>†</sup> Andreas Trügler,<sup>‡</sup> Ulrich Hohenester,<sup>‡</sup> Alfred Leitenstorfer,<sup>†</sup> and Rudolf Bratschitsch<sup>\*,†,§</sup>

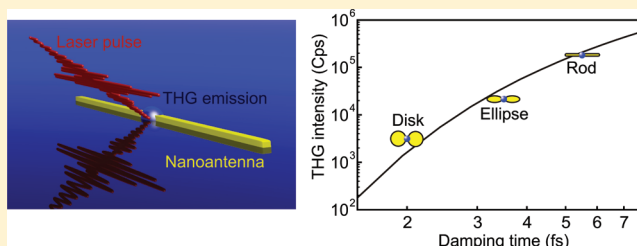
<sup>†</sup>Department of Physics and Center for Applied Photonics, University of Konstanz, D-78457 Konstanz, Germany

<sup>‡</sup>Institut für Physik, Karl-Franzens-Universität Graz, Universitätsplatz 5, 8010 Graz, Austria

## S Supporting Information

**ABSTRACT:** Plasmonic nanoantennas are efficient devices to concentrate light in spatial regions much smaller than the wavelength. Only recently, their ability to manipulate photons also on a femtosecond time scale has been harnessed. Nevertheless, designing the dynamical properties of optical antennas has been difficult since the relevant microscopic processes governing their ultrafast response have remained unclear. Here, we exploit frequency-resolved optical gating to directly investigate plasmon response times of different antenna geometries resonant in the near-infrared. Third-harmonic imaging is used in parallel to spatially monitor the plasmonic mode patterns. We find that the few-femtosecond dynamics of these nanodevices is dominated by radiative damping. A high efficiency for nonlinear frequency conversion is directly linked to long plasmon damping times. This single parameter explains the counterintuitive result that rod-type nanoantennas with minimum volume generate by far the strongest third-harmonic emission as compared to the more bulky geometries of bow-tie-, elliptical-, or disk-shaped specimens.

**KEYWORDS:** Plasmonics, nanoantennas, nonlinear optics, third-harmonic generation, frequency-resolved optical gating



Metal nanoantennas hold great promise for applications in physics, chemistry, and biology since they convert propagating light to highly localized and strongly enhanced electric fields.<sup>1–3</sup> Besides their favorable linear optical properties, nanoantennas have recently been shown to represent excellent nonlinear emitters of light.<sup>4–7</sup> In order to understand the mechanisms that govern nonlinear light emission on ultrafast time scales, steady-state characterization techniques such as two-photon photoluminescence,<sup>8–12</sup> cathodoluminescence,<sup>13</sup> dark-field scattering spectroscopy,<sup>14,15</sup> scanning near-field optical microscopy,<sup>16–18</sup> and electron energy loss spectroscopy<sup>19,20</sup> are insufficient. An extraordinary temporal resolution is required in addition to a high spatial selectivity since plasmonic effects in metal nanoantennas occur on a few-femtosecond time scale. Only recently, few-femtosecond fiber lasers became available generating pulse trains with unprecedented stability<sup>21</sup> and reaching the single-cycle limit.<sup>22</sup> Ultraprecision studies with parallel resolution at both the nanometer and femtosecond scales are enabled with these systems. Recently, we have demonstrated strong nonlinear emission from a single metal nanoantenna despite its ultrashort plasmon damping time of only a few femtoseconds.<sup>6</sup>

Here, we compare commonly used nanoantenna shapes “rod”, “ellipse”, “disk”, “bow tie”, and “cross” with respect to their nonlinear emission of light. Surprisingly, we find that the highest intensity is not linked to a specific shape, but to the smallest antenna volume. Resonant nanoantennas in the near-infrared are truly radiation-damped systems. We show that a

measurement of the few-femtosecond plasmon damping time suffices to quantify the intensity of coherent nonlinear light emission. Nonlinear imaging with subwavelength resolution reveals that the fundamental dipole mode of the plasmon is excited in all antenna types, proving them to be single-mode nanodevices.

Tailor-made arrays of gold nanoantennas are fabricated by electron beam lithography on fused silica substrates of 200  $\mu\text{m}$  thickness. They consist of two arms separated by a feedgap. Their dimensions have been carefully chosen to be exactly resonant to femtosecond excitation with linear polarization parallel to the long axis (Supporting Information, Table 1 and Figure II). Few-cycle laser pulses in the near-infrared are generated by a mode-locked erbium-doped fiber laser system working at a repetition rate of 40 MHz. The average power is typically adjusted to be 5 mW. Ultimate temporal resolution is achieved by an excitation bandwidth of 470 meV (450 nm) and using a Cassegrain reflector (NA = 0.65) for focusing. The nonlinear emission from single nanoantennas is collected in transmission geometry with a second objective (NA = 0.95), short-pass filtered (Schott BG39), dispersed with a grating monochromator (Acton Spectra Pro 2300i), and detected with a Peltier-cooled CCD camera (Andor Newton DU 920P-BU).

**Received:** November 22, 2011

**Revised:** January 9, 2012

**Published:** January 23, 2012

The most striking finding is the large intensity difference of the generated third-harmonic emission for different antenna shapes (Figure 1a). Even though all antennas are resonant for

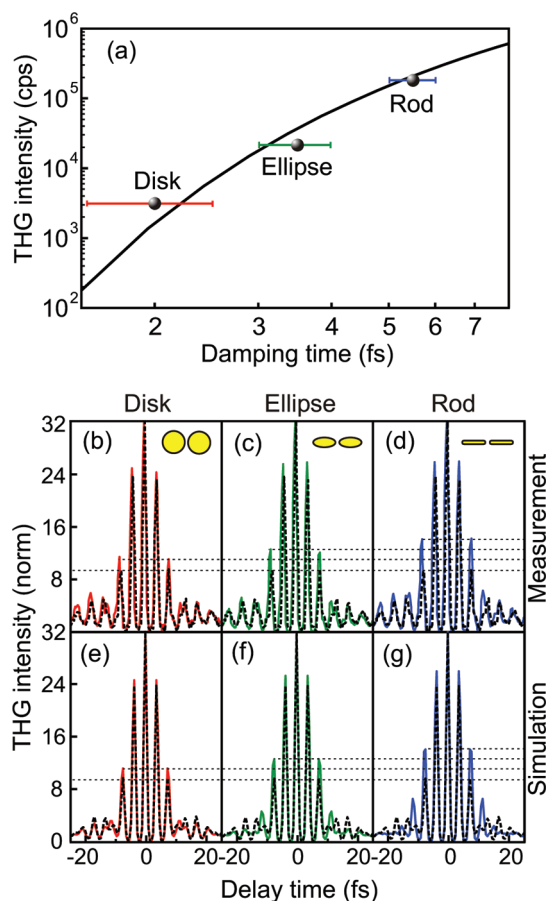


**Figure 1.** Nonlinear emission and plasmon damping from metal nanoantennas of different shapes. (a) Measured (black dots) and calculated (black line) third-harmonic intensity depending on the plasmon damping time on a logarithmic scale. (b–d) Measured and (e–g) simulated interferometric autocorrelation traces of three resonant nanoantennas, each with the autocorrelation trace of the instantaneous response from the substrate (black dashed line) shown for comparison. The rod antenna (d, g) exhibits a plasmon damping time of  $\tau = 5.5$  fs, the elliptical one (c, f) shows  $\tau = 3.5$  fs, and  $\tau = 2.0$  fs for the disk-shaped antenna (b, e). Antenna dimensions are listed in Supporting Information, Table 1.

excitation with light polarized along the long axis, the rod antenna generates 1 order of magnitude more third-harmonic intensity than the elliptical structure. Compared to the disk-shaped antenna, an increase of even 2 orders of magnitude is achieved. As we will show, the dynamical properties of the nanoantennas on the femtosecond time scale are key for understanding this phenomenon.

We use frequency-resolved optical gating at the third harmonic (THG-FROG) to measure the plasmon damping time  $\tau$  of single nanoantennas directly in the time domain.<sup>6</sup> For this purpose, we collinearly excite the structures with two identical transients derived from a Mach–Zehnder interferometer and record the emitted THG signal as a function of time delay between the pulses. Figure 1b–d shows measured THG autocorrelation traces for three different antenna shapes. The electric field amplitude and phase of the driving laser pulse

are retrieved from the THG-FROG measurement of the instantaneous response from the substrate surface. We simulate the autocorrelation traces (Figure 1e–g) by assuming harmonic oscillation of the resonant plasmon with a single-exponential decay.<sup>23</sup> The damping time constant  $\tau$  represents the only free fit parameter. It is determined by comparison of the fringe amplitudes of the measured and simulated autocorrelation data. As may be seen in Figure 1, the disk-shaped specimen exhibits the shortest plasmon dissipation time of  $\tau = 2$  fs. Note that this interval corresponds to only half a cycle of light at the fundamental resonance frequency of 250 THz. The elliptical design follows with  $\tau = 3.5$  fs. At  $\tau = 5.5$  fs, the rod antenna shows the longest storage time for the radiation energy. Weak plasmon damping is associated with an effective buildup of the plasmon oscillation, if driven on resonance. Therefore, a strong third-harmonic emission results despite the small volume of these devices. Indeed, the measured decay times may be used to calculate the relative third-harmonic intensity within the harmonic oscillator model. The excellent agreement between theory and experiment in Figure 1a clearly demonstrates that knowledge of the plasmon damping time alone suffices to predict the nonlinear emission intensity from different nanoantennas. We would like to stress that the THG emission may also be discussed in terms of near-field enhancement. Apparently, the spatially integrated plasmon damping time and the temporally integrated near-field enhancement are closely linked together. However, quantifying electric fields on the nanometer scale may almost exclusively be done by calculations. Only recently, electric near-field components in the feedgap of a single nanoantenna have been measured.<sup>24</sup> In contrast, our measurements performed in the time domain and in the far field allow for fast and reliable evaluations of the nonlinear emission from individual nanoantennas.

We now turn to the question what determines the plasmon damping time and how it can be engineered. One important issue in this context is whether the shape of the nanoantenna plays a significant role or not. It is conceivable that the excitation of differing or even multiple antenna resonances governs the observed changes in the plasmon damping time. Therefore, we analyze the plasmonic mode patterns of different nanoantenna types. Figure 2a–e shows scanning electron micrographs (SEM) of rod-, elliptical-, disk-, bow-tie-, and cross-shaped antennas. Ultimate spatial resolution is achieved for nonlinear emission mapping by replacing the Cassegrainian (NA = 0.65) by an oil immersion objective (NA = 1.3). The ultrabroadband spectrum of the pump laser is restricted to a bandwidth of 0.17 eV (225 nm) centered at 0.97 eV (1.28  $\mu\text{m}$ ). We still achieve a pulse duration as short as 24 fs in the focus of the oil immersion objective (Supporting Information, Figure III). The sample is raster-scanned within the confocal region with a step size of 50 nm and a dwell time of 50 ms. Figure 2f–p depicts spatial maps of third-harmonic emission from single gold nanoantennas of different shapes. The free-space spatial resolution of our experiment is better than the lateral extension of the subwavelength antenna structures (Supporting Information, Figure III). This performance is due to the nonlinear excitation process. Although the exact origin of the emitted photons cannot be determined in the far-field, the relevant point spread function in excitation is cubed in THG mode mapping compared to using the fundamental, which leads to the higher spatial resolution. It represents a distinct advantage over linear or lower order optical methods<sup>10,11</sup> used previously to detect higher mode patterns of single nanoantennas. Here,

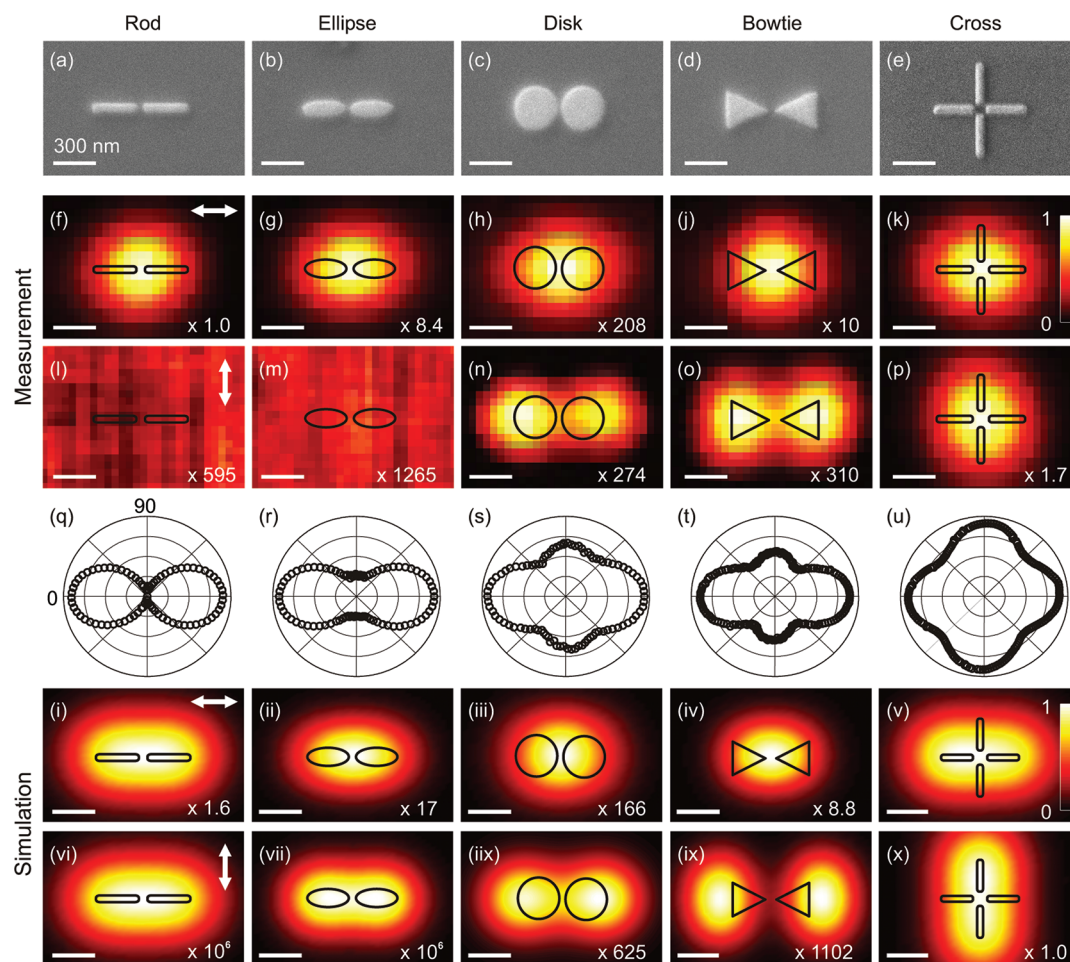


**Figure 2.** Spatially resolved third-harmonic emission from five gold nanoantennas of different shape. (a–e) Scanning electron microscope images. (f–p) Measurement. The metal nanostructures are scanned through the focus of an oil immersion objective (NA = 1.3) and excited by femtosecond laser pulses in the near-infrared. Third-harmonic emission intensity is depicted in a normalized color scale as a function of position, recorded for horizontal (f–k) and vertical (l–p) linear polarization of the excitation. (q–u) Polar plots of the third root of the measured third-harmonic intensity as a function of the polarization angle of the exciting beam. (i–x) Boundary element simulations of the third-harmonic intensity for antenna geometries as in the experiment with horizontal (i–v) and vertical (vi–x) polarization of the excitation. All scale bars are 300 nm.

we directly resolve the fundamental plasmonic mode which is accompanied by the highest field enhancement (ref 12 and Supporting Information, Figure IV). We note that this technique is also ideal for rapid systematic investigations of nanoantennas. A typical high-resolution THG map with 600 pixels and a signal-to-noise ratio better than  $10^3$  is recorded within 30 s. For linear polarization of the excitation set parallel to the resonant antenna axis (“horizontal”) the third-harmonic emission maps for all types of nanoantennas (Figure 2f–k) are found to exhibit the fundamental plasmon mode with a single hotspot in the gap region. For excitation polarized perpendicular to the main antenna axis (“vertical”) neither the rod nor the elliptical nanoantenna fulfills the resonance condition for a near-infrared plasmon. As a consequence, the residual third-harmonic emission is at least 3 orders of magnitude weaker (Figure 2l, m) compared to the horizontal configuration. The other three antenna shapes support plasmonic modes also in the vertical direction (Figure 2n–p). The third-harmonic scans for the disk- and bow-tie-shaped antennas are similar. A two-lobed pattern occurs due to the collective electron motion at the triangle bases and at the outer edges of the disks as a result of restoring Coulomb forces. The cross antenna features again one hotspot in the center. We note

that arbitrary polarizations may be converted to the near field by this antenna type provided the gap size of the antenna is sufficiently small.<sup>25</sup> The dipolar behavior of the plasmonic modes is clearly seen in the polar plots (Figure 2q–u) of the maximum signal as a function of the direction of incident linear polarization.

In order to quantitatively analyze these mode patterns, we have carried out simulations of third-harmonic emission from single nanoantennas by using a boundary element method (BEM).<sup>26,27</sup> The surface of the nanoantenna is discretized into triangles and the centroid of each triangle is taken as a collocation point where the electromagnetic fields are matched (see Supporting Information, Figure I). We use the dielectric function of gold extracted from optical data<sup>28</sup> and a refractive index of 1.35 (weighted average of substrate and air) for the embedding medium. The spatial dimensions of the metal nanostructures are analogous to the experiment (Supporting Information, Table 1 and Figure II). We consider a Gaussian excitation spot (fwhm = 300 nm) and take the third power of the electric field at the surface as source of the third-order polarizations. The coherent sum over these nonlinear dipoles then results in the third-harmonic signal. In the lower panel of Figure 2i–x, we show the calculated THG maps. The



theoretical results are almost perfectly in agreement with the corresponding experimental data above. From both experimental data and theoretical calculations of the spatial plasmonic patterns, we find that the fundamental mode is exclusively excited in all antenna types. Hence, a mechanism independent of the shape must be the reason for the different plasmon damping times and the pronounced changes in the emitted THG intensities.

To resolve this question, the basic antenna geometry is kept constant and only one antenna dimension is varied. Rod antennas with identical arm length ( $s = 260$  nm), gap distance ( $g = 50$  nm), and thickness ( $h = 30$  nm) but varying rod widths are fabricated using electron beam lithography. Figure 3a shows

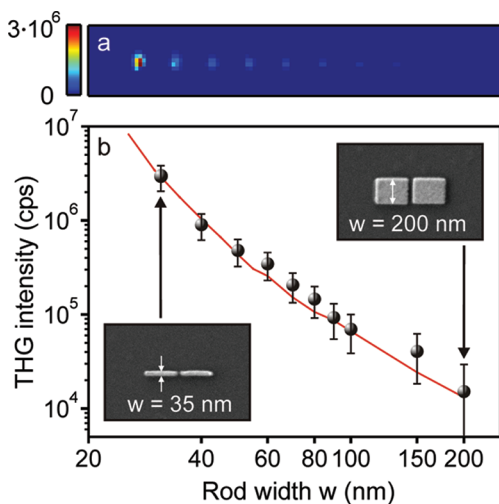


**Figure 3.** Third-harmonic emission intensity of rod nanoantennas depending on their width. (a) Color-coded third-harmonic emission scan of 10 antennas with increasing width (from left to right). (b) Extracted third harmonic emission intensity values (dots) together with BEM calculations of the emitted THG intensity (red line) on a doubly logarithmic scale. Insets: scanning electron microscope images of the narrowest (top left) and widest (bottom right) antenna, respectively. Arm length  $l = 260$  nm, structure height  $h = 30$  nm, and gap distance  $g = 50$  nm are kept constant.

the third-harmonic emission map of 10 individual rod antennas. The nanodevices are spatially separated by  $3 \mu\text{m}$  from each other. The width of the antenna arms is increasing from  $w = 35$  nm on the left image side to  $w = 200$  nm on the right. The inset of Figure 3 depicts the narrowest and the widest antenna under investigation. The extracted maximum third-harmonic intensity as a function of rod width is plotted in Figure 3b together with BEM calculations. The data clearly highlight that *high* THG light emission is directly connected to *small* antenna volumes. This observation strongly hints to radiative damping in these metal nanostructures, which is proportional to the number of coherently oscillating dipoles and therefore depending on the volume.<sup>29,30</sup>

To prove this assumption, we move back to the time domain and measure the plasmon damping times as a function of rod width of a second set of nanoantennas ( $s = 150$  nm,  $h = 20$  nm,  $g = 50$  nm). Although the variation in rod width causes a slight change of the plasmon resonance<sup>31,32</sup> (in our case the center wavelength shift of the third harmonic is 22 nm), resonant driving conditions are ensured through the large excitation bandwidth. We also verified that the pump power has no detectable effect on the damping times. The average pump

power was minimized and adjusted between 0.2 and 0.6 mW, keeping the third-harmonic intensities equally low for all antennas. As shown in Figure 4, the plasmon damping time  $\tau$

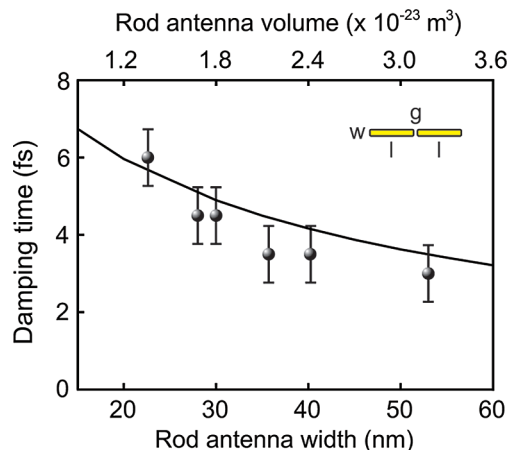


**Figure 4.** Plasmon damping time of rod nanoantennas of different widths. Measured values are depicted as dots, while the simulated values are drawn as a solid line. Nanoantenna dimensions are: arm length  $s = 150$  nm, height  $h = 20$  nm, and gap distance  $g = 50$  nm.

increases with decreasing antenna width. This damping of the fundamental plasmon oscillation directly corroborates the cubic dependence of the third-order nonlinear emission on the inverse antenna volumes from Figure 3. Simulated values for the damping times  $\tau$  in Figure 4 are gained by using the relation  $\tau = (2\pi\Delta\nu)^{-1}$ , where the homogeneous line width  $\Delta\nu$  is extracted from scattering spectra calculated with the BEM method for exactly the same antenna geometries. The measured damping times quantitatively agree with simulated ones, which finally proves that our infrared nanoantennas with volumes between  $1.4 \times 10^{-22}$  and  $3.4 \times 10^{-21}$  m<sup>3</sup> are indeed dominated by radiative damping. Given that this is a purely dissipative process, we always discuss the energy relaxation time  $\tau$ . Under our conditions,  $\tau$  is directly linked to the dephasing time  $T_2$  of the oscillation amplitude<sup>23,33</sup> via  $T_2 = 2\tau$ . We would like to note that for gold nanorods with volumes below  $0.6 \times 10^{-22}$  m<sup>3</sup> and resonant in the adjacent *visible* range damping was attributed to electronic interband transitions.<sup>14</sup> Only for small probed volumes and at higher plasmon energies, loss mechanisms such as carrier–carrier, carrier–lattice, and surface scattering become increasingly important.<sup>34,35</sup> In the near-infrared, however, metal antennas are limited solely by the process they are intended for, namely radiation coupling.

In conclusion, we have presented nonlinear emission spectroscopy as a powerful tool to characterize and design single metal nanoantennas in space and time. On the temporal scale, few-femtosecond plasmon damping times are directly measured for different antenna shapes. Because of radiative damping, the lowest antenna volumes generate by far the strongest third-harmonic emission. On the spatial scale, the third-harmonic emission of different types of nanoantennas is mapped out to prove operation at the fundamental mode. By combining subwavelength concentration in space with few-cycle response times, the ultimate focusing of light has been demonstrated in all four dimensions. Our findings provide design capabilities for nanoantennas (or plasmonic nanostructures in general) with either an ultrabroadband spectral coverage or low radiative damping rates accompanied by

maximum nonlinear efficiencies.<sup>36</sup> This knowledge will also be decisive for the creation of tailored hybrid antenna–nano-emitter systems<sup>37</sup> for applications in few-photon quantum optics on a femtosecond time scale.<sup>38</sup>

## ■ ASSOCIATED CONTENT

### 📄 Supporting Information

Additional tables and figures. This material is available free of charge via the Internet at <http://pubs.acs.org>.

## ■ AUTHOR INFORMATION

### Corresponding Author

\*E-mail: [Rudolf.Bratschitsch@physik.tu-chemnitz.de](mailto:Rudolf.Bratschitsch@physik.tu-chemnitz.de).

### Present Address

§Institute of Physics, Chemnitz University of Technology, D-09107 Chemnitz, Germany.

## ■ REFERENCES

- (1) Crozier, K. B.; Sundaramurthy, A.; Kino, G. S.; Quate, C. F. Optical Antennas: Resonators for Local Field Enhancement. *J. Appl. Phys.* **2003**, *94*, 4632.
- (2) Ozbay, E. Plasmonics: Merging Photonics and Electronics at Nanoscale Dimensions. *Science* **2006**, *311*, 189.
- (3) Bharadwaj, P.; Deutsch, B.; Novotny, L. Optical Antennas. *Adv. Opt. Photonics* **2009**, *1*, 438.
- (4) Danckwerts, M.; Novotny, L. Optical Frequency Mixing at Coupled Gold Nanoparticles. *Phys. Rev. Lett.* **2007**, *98*, 026104.
- (5) Kim, S.; et al. High-Harmonic Generation by Resonant Plasmon Field Enhancement. *Nature* **2008**, *453*, 757.
- (6) Hanke, T.; et al. Efficient Nonlinear Light Emission of Single Gold Optical Antennas Driven by Few-Cycle Near-Infrared Pulses. *Phys. Rev. Lett.* **2009**, *103*, 257404.
- (7) Ko, K. D.; et al. Nonlinear Optical Response from Arrays of Au Bowtie Nanoantennas. *Nano Lett.* **2010**, *11*, 61.
- (8) Mühlischlegel, P.; Eisler, H.-J.; Martin, O. J. F.; Hecht, B.; Pohl, D. W. Resonant Optical Antennas. *Science* **2005**, *308*, 1607.
- (9) Schuck, P. J.; Fromm, D. P.; Sundaramurthy, A.; Kino, G. S.; Moerner, W. E. Improving the Mismatch between Light and Nanoscale Objects with Gold Bowtie Nanoantennas. *Phys. Rev. Lett.* **2005**, *94*, 017402.
- (10) Beermann, J.; Novikov, S. M.; Sondergaard, T.; Boltasseva, A.; Bozhevolnyi, S. I. Two-Photon Mapping of Localized Field Enhancements in Thin Nanostrip Antennas. *Opt. Express* **2008**, *16*, 17302.
- (11) Ghenuche, P.; Cherukulappurath, S.; Taminiau, T. H.; van Hulst, N. F.; Quidant, R. Spectroscopic Mode Mapping of Resonant Plasmon Nanoantennas. *Phys. Rev. Lett.* **2008**, *101*, 116805.
- (12) Huang, J.-S.; et al. Mode Imaging and Selection in Strongly Coupled Nanoantennas. *Nano Lett.* **2010**, *10*, 2105.
- (13) Vesseur, E. J. R.; de Waele, R.; Kuttge, M.; Polman, A. Direct Observation of Plasmonic Modes in Au Nanowires Using High-Resolution Cathodoluminescence Spectroscopy. *Nano Lett.* **2007**, *7*, 2843.
- (14) Sönnichsen, C.; et al. Drastic Reduction of Plasmon Damping in Gold Nanorods. *Phys. Rev. Lett.* **2002**, *88*, 077402.
- (15) Merlein, J.; et al. Nanomechanical Control of an Optical Antenna. *Nature Photonics* **2008**, *2*, 230.
- (16) Esteban, R.; et al. Direct Near-Field Optical Imaging of Higher Order Plasmonic Resonances. *Nano Lett.* **2008**, *8*, 3155.
- (17) Jones, A. C.; et al. Mid-IR Plasmonics: Near-Field Imaging of Coherent Plasmon Modes of Silver Nanowires. *Nano Lett.* **2009**, *9*, 2553.
- (18) Schnell, M.; et al. Amplitude- and Phase-Resolved Near-Field Mapping of Infrared Antenna Modes by Transmission-Mode Scattering-Type Near-Field Microscopy. *J. Phys. Chem. C* **2010**, *114*, 7341.
- (19) Nelayah, J.; et al. Mapping Surface Plasmons on a Single Metallic Nanoparticle. *Nature Phys.* **2007**, *3*, 348.
- (20) Schaffer, B.; Hohenester, U.; Trügler, A.; Hofer, F. High Resolution Surface Plasmon Imaging of Gold Nanoparticles by Energy Filtered Transmission Electron Microscopy. *Phys. Rev. B* **2009**, *79*, 041401.
- (21) Sell, A.; Krauss, G.; Scheu, R.; Huber, R.; Leitenstorfer, A. 8-fs Pulses from a Compact Er:Fiber System: Quantitative Modeling and Experimental Implementation. *Opt. Express* **2009**, *17*, 1070.
- (22) Krauss, G.; et al. Synthesis of a Single Cycle of Light with Compact Erbium-Doped Fibre Technology. *Nature Photonics* **2010**, *4*, 33.
- (23) Lamprecht, B.; Krenn, J. R.; Leitner, A.; Aussenegg, F. R. Resonant and Off-Resonant Light-Driven Plasmons in Metal Nanoparticles Studied by Femtosecond-Resolution Third-Harmonic Generation. *Phys. Rev. Lett.* **1999**, *83*, 4421.
- (24) Schnell, M.; Garcia-Etxarri, A.; Alkorta, J.; Aizpurua, J.; Hillenbrand, R. Phase-Resolved Mapping Of the Near-Field Vector and Polarization State in Nanoscale Antenna Gaps. *Nano Lett.* **2010**, *10*, 3524.
- (25) Biagioni, P.; Huang, J. S.; Duo, L.; Finazzi, M.; Hecht, B. Cross Resonant Optical Antenna. *Phys. Rev. Lett.* **2009**, *102*, 256801.
- (26) Garcia de Abajo, F. J.; Howie, A. Retarded Field Calculation of Electron Energy Loss in Inhomogeneous Dielectric. *Phys. Rev. B* **2002**, *65*, 115418.
- (27) Hohenester, U.; Trügler, A. MNPBEM - A Matlab Toolbox for the Simulation of Plasmonic Nanoparticles. *Comput. Phys. Commun.* **2012**, *183*, 370.
- (28) Johnson, P. B.; Christy, R. W. Optical Constant of Noble Metals. *Phys. Rev. B* **1972**, *6*, 4370–4379.
- (29) Crowell, J.; Ritchie, R. H. Radiative Decay of Coulomb-Stimulate Plasmons in Spheres. *Phys. Rev.* **1968**, *172*, 436–440.
- (30) Wokaun, A.; Gordon, J. P.; Liao, P. F. Radiation Damping in Surface-Enhanced Raman Scattering. *Phys. Rev. Lett.* **1982**, *48*, 957.
- (31) Novotny, L. Effective Wavelength Scaling for Optical Antennas. *Phys. Rev. Lett.* **2007**, *98*, 266802.
- (32) Bryant, G. W.; Garcia de Abajo, F. J.; Aizpurua, J. Mapping the Plasmon Resonances of Metallic Nanoantennas. *Nano Lett.* **2008**, *8*, 631.
- (33) Stietz, F.; et al. Decay Times of Surface Plasmon Excitation in Metal Nanoparticles by Persistent Spectral Hole Burning. *Phys. Rev. Lett.* **2000**, *84*, S644.
- (34) Klar, T.; et al. Surface-Plasmon Resonances in Single Metallic Nanoparticles. *Phys. Rev. Lett.* **1998**, *80*, 4249.
- (35) Anderson, A.; Deryckx, K. S.; Xu, X. G.; Steinmeyer, G.; Raschke, M. B. Few-Femtosecond Plasmon Dephasing of a Single Metallic Nanostructure from Optical Response Function Reconstruction by Interferometric Frequency Resolved Optical Gating. *Nano Lett.* **2010**, *10*, 2519.
- (36) Park, I.-Y.; et al. Plasmonic Generation of Ultrashort Extreme-Ultraviolet Light Pulses. *Nature Photonics* **2011**, *5*, 677.
- (37) Rogobete, L.; Kaminski, F.; Agio, M.; Sandoghdar, V. Design of Plasmonic Nanoantennae for Enhancing Spontaneous Emission. *Opt. Lett.* **2007**, *32*, 1623.
- (38) Sotier, F.; et al. A Femtosecond Few-Fermion Dynamics and Deterministic Single-Photon Gain in a Quantum Dot. *Nature Phys.* **2009**, *5*, 352.